

Barotropic instability in the tropical cyclone outer region

Jiayi Peng,^{a*} Tim Li,^{a,b} Melinda S. Peng^{c †} and Xuyang Ge^a

^a*International Pacific Research Center, University of Hawaii at Manoa, Honolulu, Hawaii, USA*

^b*Department of Meteorology, University of Hawaii at Manoa, Honolulu, Hawaii, USA*

^c*Naval Research Laboratory, Monterey, California, USA*

ABSTRACT: The growth of asymmetric perturbations and their interactions with the symmetric flow are investigated for wind profiles in a tropical cyclone with instability in its outer region. Three tangential wind profiles are examined: TC1, a strong barotropic instability profile in the outer region; TC2, a stable wind profile; and TC3, a weaker instability profile comparing to TC1 with a larger distance between the inner negative and the outer positive vorticity gradient centres.

An eigenvalue analysis indicates that azimuthal wave-number two is the most unstable mode in both TC1 and TC3, with an e-folding time-scale of about 1 and 9 days, respectively. Numerical simulations using a linear barotropic model, with an initial asymmetry specified in the outer region, confirm the eigenvalue analysis. A mechanism is provided to explain the difference between simulations in TC1 and TC2. In both the stable and unstable case, an inner asymmetry is induced by the initial outer asymmetry acting on the symmetric vorticity gradient. Subsequently, the newly generated inner asymmetry feeds back positively to the outer asymmetry with the unstable profile. Because of this positive feedback, the inner and the outer asymmetries maintain an up-shear phase tilting, leading to a continuous energy transfer from the symmetric flow to the asymmetric perturbation. In the stable TC2, the inner asymmetry could not amplify the outer initial asymmetry as there is no basic-state radial vorticity gradient there. Also due to this feedback process, disturbances grow faster where the (absolute) basic-state vorticity gradients are large. Therefore, the position of an initial disturbance plays a minor role in determining the outcome of the system.

Simulations with a nonlinear barotropic model and a primitive equation model further confirm the significant weakening of the maximum tangential wind due to the positive feedback process in TC1. Simulations for TC3 show a smaller change of the symmetric tangential wind, as expected. Copyright © 2009 Royal Meteorological Society

KEY WORDS tropical cyclone intensity; asymmetric perturbations; barotropic instability

Received 14 August 2008; Revised 15 February 2009; Accepted 23 February 2009

1. Introduction

The stability analysis of discrete modes in symmetric vortices is a topic of broad interest. Barotropic instability was suggested by Staley and Gall (1979) as a possible mechanism for destructive suction spots imbedded within tornados. Gent and McWilliams (1986) examined several different ocean current profiles for instability using the quasi-geostrophic potential vorticity equation and found that the most unstable mode can be internal or external, depending on the sharpness of the wind profile. Observational and model studies (e.g. Möller and Smith, 1994) show that a tropical cyclone (TC) may have an annular ring of high potential vorticity (PV) with low PV in the central region. Concentric eyewall patterns are frequently observed in radar reflectivity (Black and Willoughby, 1992). Deep convection within the inner eyewall (large vorticity region) is surrounded by a nearly

echo-free moat (low vorticity region), and further surrounded by an outer ring of deep convection (relatively enhanced vorticity region). The reversal of the radial PV gradient near an eyewall might cause barotropic instability (Montgomery and Shapiro, 1995). The stability in an annular vorticity region, representing an eyewall, was examined within the framework of a linear and nonlinear barotropic non-divergent model (Schubert *et al.*, 1999). Polygonal eyewalls are shown to form as a result of barotropic instability near the radius of maximum winds (RMW). Kossin *et al.* (2000) investigated both the instability across the outer ring of enhanced vorticity and the instability across the moat. The former occurs when the outer ring is sufficiently narrow and the circulation of the central vortex is sufficiently weak. The latter occurs when the radial extent of the moat is sufficiently narrow so that a positive feedback may occur between the central vortex and the inner edge of the ring.

Most previous studies were focused on the instability near the TC inner eyewall region (e.g. Nolan and Montgomery, 2000, 2002; Kossin and Schubert, 2001; Nolan *et al.*, 2001; Terwey and Montgomery, 2002; Nolan and Grasso, 2003). However, recent singular vector (SV) diagnostics by Peng and Reynolds (2006) indicate that the

*Correspondence to: Jiayi Peng, International Pacific Research Center, University of Hawaii at Manoa, 1680 East West Road, Honolulu, HI 96822, USA.

E-mail: pengj@hawaii.edu

†The contribution of Melinda S. Peng to this article was prepared as part of her official duties as a United States Federal Government Employee.

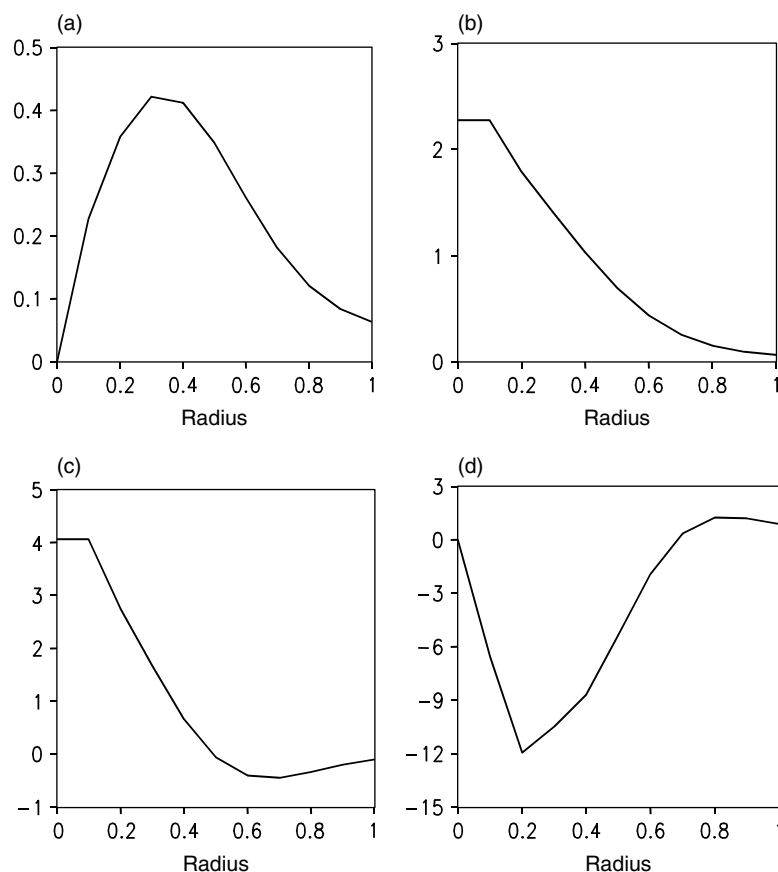


Figure 1. Radial (unit: 1000 km) profiles of the symmetric TC vortex from NOGAPS analysis for hurricane Isabel on 10 September 2003: (a) tangential wind (unit: 50 m s^{-1}), (b) angular velocity (unit: $5 \times 10^{-5} \text{ s}^{-1}$), (c) vorticity (unit: $5 \times 10^{-5} \text{ s}^{-1}$), and (d) vorticity gradient (unit: $5 \times 10^{-11} \text{ m}^{-1} \text{ s}^{-1}$).

TC intensity forecasts are most sensitive to the initial state where the PV gradient changes sign in the outer region, located roughly 500 to 700 km away from the TC centre (an example is given in Figure 1). This sign change represents a necessary condition for the barotropic instability (Rayleigh, 1880) in the outer region. The SV analysis suggests a possible new energy source/sink for TC intensity changes, that is, the unstable growth of perturbations associated with the instability in the outer region. This study is dedicated to a theoretical investigation of how asymmetric perturbations can grow under this type of unstable mean profile and modify the mean state. We will explore the specific process that causes the energy transfer from the symmetric mean flow to the asymmetric perturbation, as well as the interaction between the perturbation and the symmetric mean flow.

The paper is organized as follows. Section 2 contains the eigenvalue stability analysis for three different TC wind profiles. In section 3, we discuss the dynamic processes associated with asymmetric perturbation growth based on the analysis of a linear non-divergent barotropic model simulation. Nonlinear non-divergent barotropic model simulations are discussed in section 4. Section 5 describes the results from a three-dimensional full physics model. Simulations with initial disturbances placed at different radial positions are discussed in section 6. The investigation for an unstable profile with a smaller scale

is discussed in section 7. Conclusion and discussion are given in section 8.

2. Linear stability analysis

The SV analysis by Peng and Reynolds (2006) indicates that the intensity forecast of a TC is most sensitive to initial conditions at regions where the PV gradient changes sign. An example is given in Figure 1 from the Navy Operational Global Atmospheric Prediction System (NOGAPS) analysis for hurricane Isabel on 10 September 2003. This vortex profile satisfies the necessary condition for barotropic instability (Rayleigh, 1880). An analytic expression is constructed to approximate the observed wind profile with the following mathematic formula, specified by the symmetric vorticity gradient:

$$\frac{\partial \bar{\zeta}}{\partial r} = a_1 \exp[-0.5 \times \{(r - r_1)/0.08\}^2] + a_2 \exp[-0.5 \times \{(r - r_2)/0.08\}^2], \quad (2.1)$$

where r is the radial distance. Three different profiles are investigated with different specifications of a_1 , a_2 , r_1 and r_2 , where r_1 and r_2 determine the positions of the minimum and maximum and a_1 and a_2 determine their magnitudes. For TC1 (Figure 2, solid line), $a_1 = -40.0$ and $a_2 = 6.0$, that give the minimum vorticity gradient at

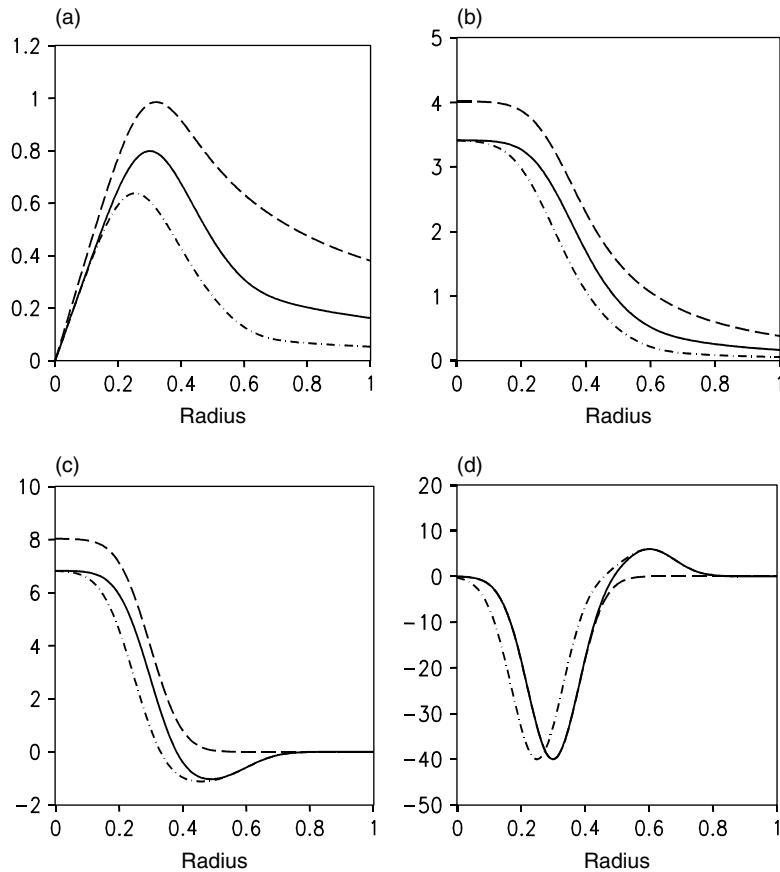


Figure 2. Radial profiles of the idealized vortices for non-dimensional (a) tangential wind, (b) angular velocity, (c) vorticity, and (d) vorticity gradient for TC1 (solid), TC2 (dashed) and TC3 (dash-dotted line).

$r_1 = 0.3$ and the maximum vorticity gradient at $r_2 = 0.6$. There is a sign change of the vorticity gradient near the radius of 0.5. For TC2, $a_2 = 0.0$, so that there is no sign change in the radial vorticity gradient and it corresponds to a stable profile (Figure 2, dashed line). For TC3, all parameters are the same as TC1 except $r_1 = 0.25$. This results in a larger distance between the locations of the minimum and maximum vorticity gradient centres and a smaller vorticity gradient (Figure 2(d), dash-dotted line). TC1 has a maximum non-dimensional tangential wind of 0.80 (or a dimensional value of 40 m s^{-1}) located at the radius of 0.3 (300 km); TC2 has a maximum tangential wind of 1.0 (50 m s^{-1}) situated at the radius of 0.3 (300 km); and TC3 has a maximum tangential wind of 0.64 (32 m s^{-1}) at the radius of 0.25 (250 km).

The instability of the three symmetric wind profiles is examined with the eigenvalue analysis of a linear non-divergent barotropic vorticity equation. The time tendency of the perturbation stream function $\psi'(r, \lambda, t)$ in cylindrical coordinates is governed by:

$$\left(\frac{\partial}{\partial t} + \bar{v} \frac{\partial}{r \partial \lambda} \right) \nabla^2 \psi' - \frac{\partial \psi'}{r \partial \lambda} \frac{d\bar{\zeta}}{dr} = 0, \quad (2.2)$$

where $\bar{v}(r)$ is the basic-state (symmetric) tangential wind, $\bar{\zeta}(r) = d(r\bar{v})/rdr$ is the basic-state relative vorticity, $(u', v') = (-\partial\psi'/r\partial\lambda, \partial\psi'/\partial r)$ is the perturbation radial and tangential wind, and $\zeta' = \nabla^2\psi' = \partial(rv')/r\partial r -$

$\partial u'/r\partial\lambda$ is the perturbation vorticity. Assume that the perturbation stream function has a solution in the form of $\psi'(r, \lambda, t) = \hat{\psi}(r)e^{i(k\lambda - \omega t)}$, where k is the azimuthal wave number and ω the complex frequency, we obtain from (2.2) an ordinary differential equation for $\hat{\psi}(r)$:

$$\left\{ r \frac{d}{dr} \left(r \frac{d\hat{\psi}}{dr} \right) - k^2 \hat{\psi} \right\} \omega = k \frac{\bar{v}}{r} \left\{ r \frac{d}{dr} \left(r \frac{d\hat{\psi}}{dr} \right) - k^2 \hat{\psi} \right\} - kr \frac{d\bar{\zeta}}{dr} \hat{\psi}, \quad (2.3)$$

where $\omega = a + bi$. For a given wave number k , $b > 0$ denotes that this wave is unstable and the non-dimensional growth rate is b . To solve (2.3), a central difference is applied to approximate the radial derivatives, with vanishing stream function and its gradient as the boundary conditions at the radial end points.

Figure 3(a) shows the growth rate as a function of the wave number for the three radial wind profiles, TC1, TC2, and TC3. As expected, the TC2 profile is stable. For TC1, the wave-number two is unstable with a growth rate $b = 0.21283$, corresponding to an e-folding time-scale of 26 hours. A weaker wave-number two instability is found in TC3, with a growth rate $b = 0.02590$ and the e-folding time-scale of 215 hours.

In TC1, the most unstable mode has a maximum located at $r = 0.3$ where the (absolute) maximum vorticity gradient is located, and a second, much weaker,

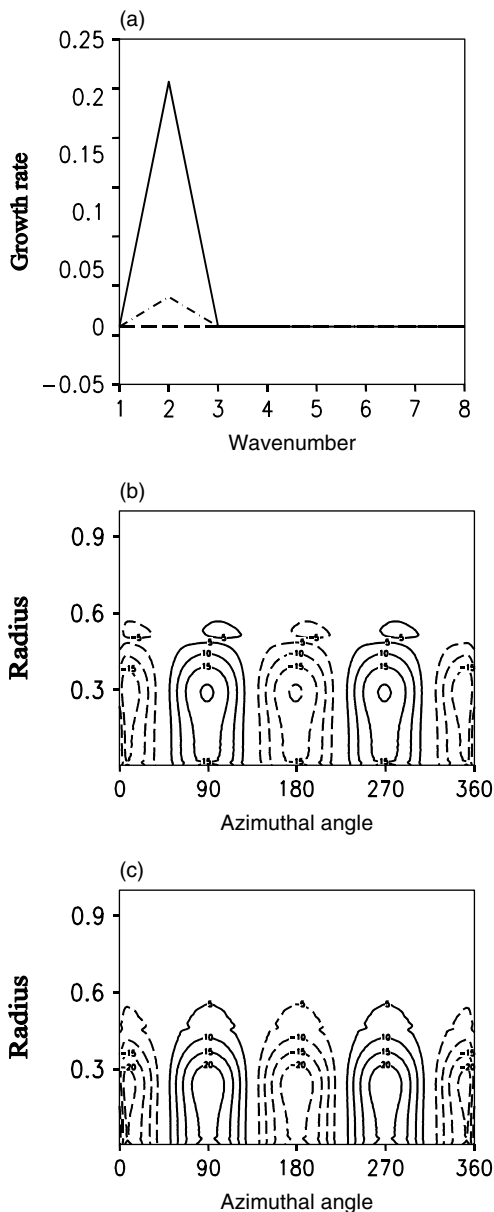


Figure 3. (a) Growth rates as a function of wave number for TC1 (solid line), TC2 (dashed line) and TC3 (dash-dotted line) and the vorticity patterns of the most unstable mode for (b) TC1 and (c) TC3.

maximum located at $r = 0.55$ (Figure 3(b)). In TC3, the locations of the maxima are slightly inward than in TC1. The result suggests that, even if the unstable profile is in the outer region, the asymmetric perturbation develops most rapidly in the inner region near the maximum negative vorticity gradient centre.

3. Linear barotropic model simulations

Schubert *et al.* (1999) and Kossin *et al.* (2000) have the analytic solution for a given piecewise-constant vorticity profile for a TC-like vortex with the instability near the TC inner core region. The eigenvalue analysis we carried out for instability in the TC outer region indicates an unstable growth of the asymmetric perturbation, with its maximum growth near the radius of the maximum

wind. How does a rather weak outer instability lead to the growth of inner asymmetries? This motivates us to further conduct linear non-divergent barotropic model simulations to understand how the asymmetric perturbation gains energy from the symmetric vortex.

The governing equations for a linear non-divergent barotropic model on an f -plane ($f = 5 \times 10^{-5} \text{ s}^{-1}$) are:

$$\left. \begin{aligned} \frac{\partial u'}{\partial t} + \bar{u} \frac{\partial u'}{\partial x} + \bar{v} \frac{\partial u'}{\partial y} + u' \frac{\partial \bar{u}}{\partial x} + v' \frac{\partial \bar{u}}{\partial y} - v' &= -\frac{\partial \phi'}{\partial x}, \\ \frac{\partial v'}{\partial t} + \bar{u} \frac{\partial v'}{\partial x} + \bar{v} \frac{\partial v'}{\partial y} + u' \frac{\partial \bar{v}}{\partial x} + v' \frac{\partial \bar{v}}{\partial y} + u' &= -\frac{\partial \phi'}{\partial y}, \\ \frac{\partial}{\partial x} \left(\bar{u} \frac{\partial u'}{\partial x} + \bar{v} \frac{\partial u'}{\partial y} + u' \frac{\partial \bar{u}}{\partial x} + v' \frac{\partial \bar{u}}{\partial y} \right) &+ \frac{\partial}{\partial y} \left(\bar{u} \frac{\partial v'}{\partial x} + \bar{v} \frac{\partial v'}{\partial y} + u' \frac{\partial \bar{v}}{\partial x} + v' \frac{\partial \bar{v}}{\partial y} \right) - \zeta' = -\nabla^2 \phi', \end{aligned} \right\} \quad (3.1)$$

where u and v are the zonal and meridional wind components, ϕ the geopotential height, and ζ the relative vorticity. Variables with an overbar represent the basic state and those with a prime are perturbations.

All model variables have been non-dimensionalized with a characteristic time-scale of $T = 1/f = 2 \times 10^4 \text{ s}$ (a non-dimensional time $t = 0.18$ corresponds to 1 hour) and characteristic velocity and horizontal length scale of $C = 50 \text{ m s}^{-1}$ and $L = CT = 1000 \text{ km}$, respectively. The numerical technique employed includes a fourth-order Runge–Kutta time-integration scheme with a time increment of 0.002 (40 s), a Matsuno advection scheme (Shen *et al.*, 2003), and a second-order central difference scheme for space derivatives. The model covers a 4 by 4 (4000 km by 4000 km) domain with a grid resolution of 0.004 (4 km) in both x and y directions. The lateral boundary condition is a radiative boundary. All the simulations are carried out to time 8.64 (48 hours). Most of the results shown are up to 4.32 (24 hours) during which wave–mean flow interactions occur.

The three symmetric tangential wind profiles, TC1, TC2 and TC3 as specified in section 2 (Figure 2(a)), are investigated. An initial wave-number two asymmetric perturbation is introduced with the following structure:

$$\zeta' = A \times \exp\{-0.5 \times (10r - 6)^2\} \cos(2\lambda), \quad (3.2)$$

where r is the radial distance, λ the azimuthal angle, and A the amplitude of the perturbations. The maximum of the perturbation is placed at the radius of 0.6 (600 km) in the outer region of the TC. A modest initial perturbation, $A = 0.5$, is specified. This corresponds to a perturbation vorticity that is 7.4% of the basic-state maximum vorticity. All model outputs are interpolated to a cylindrical coordinate system about the vortex centre and they are decomposed into a symmetric and an asymmetric component for further diagnosis.

The temporal evolution of both the asymmetric vorticity amplitude and asymmetric kinetic energy (KE) for the three experiments are displayed in Figure 4. Although

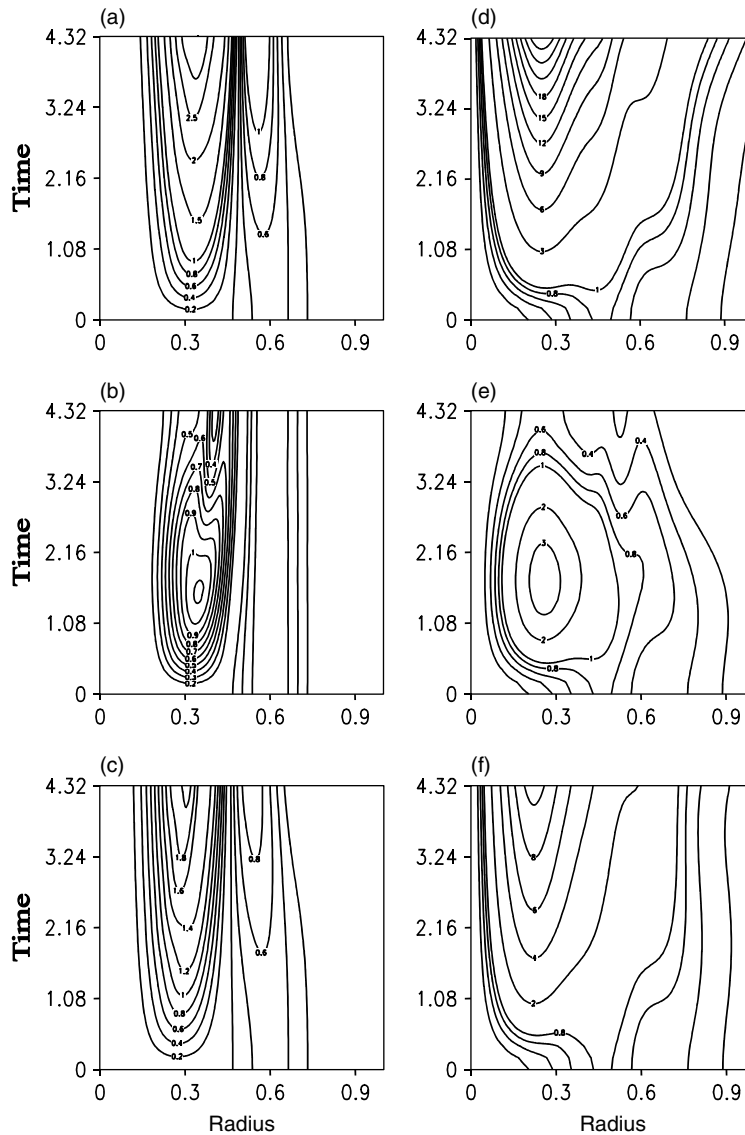


Figure 4. The time–radius cross-section of the wave-number two vorticity amplitude (left panels) and the asymmetric kinetic energy (right panels) in the linear barotropic model experiments for TC1 (top), TC2 (middle) and TC3 (bottom).

the initial perturbation is located at $r = 0.6$, the maximum growth of the asymmetric perturbation in TC1 is situated at the inner region (near $r = 0.3$), where the negative vorticity gradient is the largest (see Figure 2(d), solid line). The non-dimensional growth rate in the inner region is 0.3, which corresponds to an e-folding time-scale of 18 hours. The location of maximum growth and the growth rate agree well with the eigenvalue analysis in the previous section. The evolution of the asymmetry in TC3 is very similar to the one in TC1, except with a smaller growth. While the asymmetric perturbations continue to grow in the unstable profiles TC1 and TC3, the inner asymmetry in the stable TC2 grows initially and then decays and the outer asymmetry has little change (Peng *et al.*, 2008).

The cause for the growth of new asymmetry inside the initially specified asymmetry is due to the interaction between the initial perturbation radial wind and the basic vorticity gradient, while its subsequent decay under

a stable symmetric wind profile (such as TC2) is due to vortex axisymmetrization as studied previously by Montgomery and Kallenbach (1997) and Peng *et al.* (2008). In a vortex with differential rotation, an up-shear tilting of the perturbation would lead to an energy transfer from the symmetric vortex to the asymmetric perturbation, while a down-shear tilting would lead to an opposite energy transfer. Figure 5 illustrates the evolution of the asymmetric vorticity pattern (shaded area) in TC2, plotted in the radial and azimuthal coordinates for better viewing of the phase tilt. A phase line is defined by connecting the inner and outer asymmetric vorticity centres, and a line parallel to the radial axis has no phase tilt with respect to the tangential wind shear (note that the angular velocity decreases monotonically with radius (Figure 2(b))). Initially, an outer vorticity perturbation is introduced at $r = 0.6$. Quickly, an asymmetric perturbation develops in the inner region with its maximum located at $r = 0.3$ where the basic vorticity gradient is largest. At $t = 0.54$,

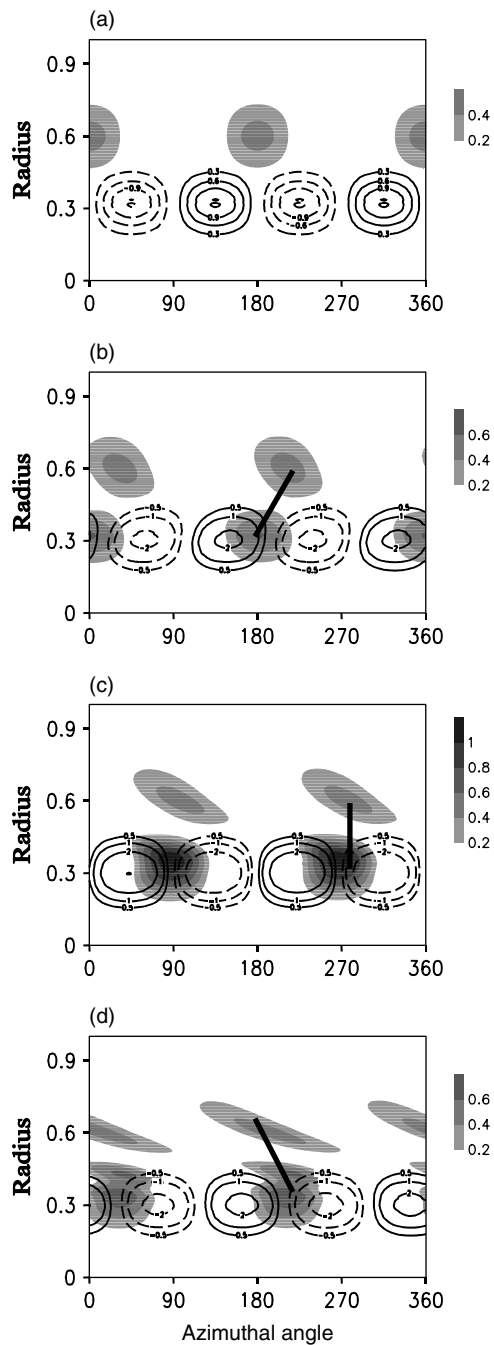


Figure 5. The asymmetric vorticity pattern (positive only, shaded) and the vorticity advection by asymmetric flow (contour) at time (a) 0.0, (b) 0.54, (c) 1.62, and (d) 3.24 in linear barotropic experiment for TC2. The thick line represents the phase tilting of the asymmetric perturbations. An increasing azimuthal angle is downstream for the basic cyclonic flows.

there is a clear up-shear tilting. The phase line changes to a down-shear tilting by $t = 3.24$. The change of the tilting from up-shear to neutral and then to down-shear corresponds well to the time tendency of the perturbation energy (Figure 4(e)).

The time tendency of the asymmetric barotropic vorticity can be written as

$$\frac{\partial \zeta'}{\partial t} = -\frac{\bar{v}}{r} \frac{\partial \zeta'}{\partial \lambda} - u' \frac{\partial \bar{\zeta}}{\partial r}. \quad (3.3)$$

Here, u' is the asymmetric radial wind, \bar{v} the basic-state tangential wind, ζ' the asymmetric vorticity, and $\bar{\zeta}$ the symmetric vorticity. The first term on the right-hand side represents the vorticity advection by the symmetric mean flow. This term does not cause the growth of the asymmetric vorticity, and instead, only redistributes the initial asymmetric vorticity that would contribute to its phase change. The second term on the right-hand side represents the mean vorticity advection by the asymmetric radial wind. This term, as shown in Figure 5 (contour line), is responsible for the generation of the new vorticity perturbation and the initial up-shear tilting of the total asymmetry. As the inner asymmetry develops, the vorticity advection by the symmetric angular velocity, which is faster (slower) in the inner (outer) region, causes the transition of the asymmetry tilt from up-shear to neutral and further to down-shear. Detailed discussion on the phase change for stable profiles is given in Peng *et al.* (2008).

The time snapshots of the asymmetry for the unstable TC1 are depicted in Figure 6. Unlike TC2, the asymmetry always keeps an up-shear tilt even under basic-state differential rotation. This implies that the asymmetric perturbation will always gain energy from the symmetric mean flow, as shown in Figure 4(d). Note that in TC1, a positive vorticity gradient exists in the outer region (which does not exist in TC2) so that u' associated with the inner asymmetry can feed back positively to the outer asymmetry, and the outer asymmetry further feed into the inner asymmetry. Through this continuous two-way positive feedback process, both the inner and outer asymmetric perturbations grow by gaining energy from the symmetric flow.

Figure 7 shows the evolution of the asymmetric radial wind and the vorticity advection by the asymmetric flow (the second term in (3.3)) in both the inner and outer regions. Consistent with the up-shear tilting pattern (i.e. the outer perturbation is always located on the downstream side of the inner perturbation), the asymmetric radial wind remains as positive (negative) in the inner (outer) region all the time (Figure 7(a)). This radial wind distribution causes positive vorticity tendencies in both the inner and outer regions (Figure 7(b)), as the basic-state vorticity gradient is negative in the inner region and positive in the outer region (Figure 2(d), solid line). The time changing-rate of the asymmetric vorticity in the inner region is greater than that in the outer region, primarily because the amplitude of the inner negative symmetric vorticity gradient is about 7 times greater than that of the outer positive vorticity gradient. The total vorticity change is similar to the vorticity advection by the asymmetric flow (figure not shown).

The diagnosis of the asymmetric vorticity budget indicates that the maintenance of the up-shear tilting comes primarily from the second advection term in (3.3). The inner core asymmetry rotates faster than the outer asymmetry due to the advection by the symmetric mean angular velocity (the first term in (3.3)). However, the advection by the asymmetric radial wind generates a maximum vorticity tendency downstream in the outer

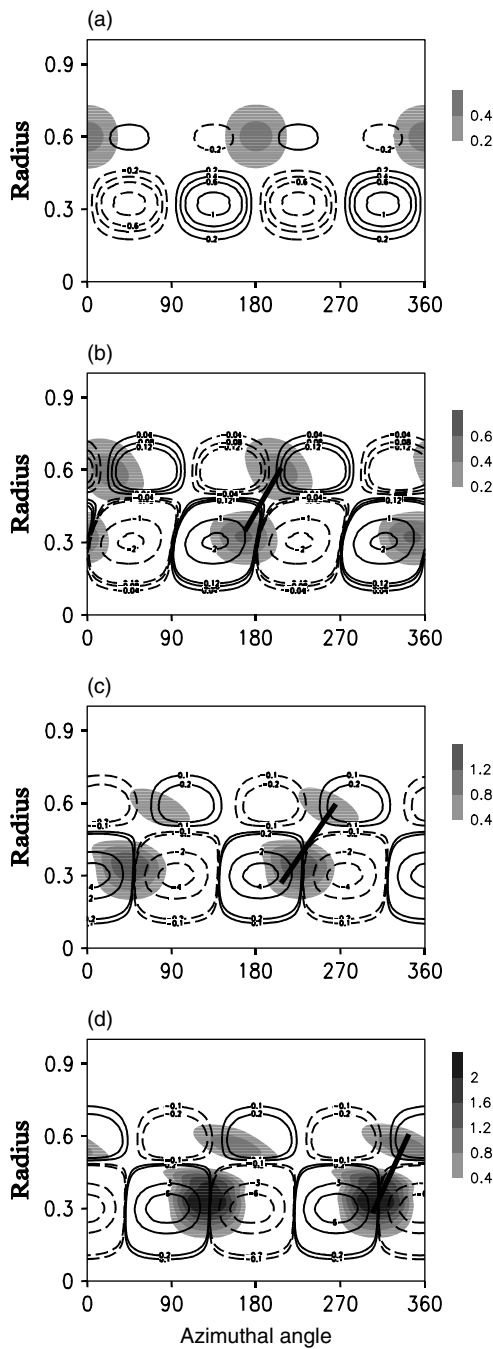


Figure 6. Same as Figure 5 except for TC1.

region (Figure 8(a)) and a maximum vorticity tendency upstream in the inner region (Figure 8(b)). This offsets the effect of differential rotation by the mean flow (part of axisymmetrization). As a result, the up-shear tilting of the asymmetry is kept, which can be clearly seen from the phase between the inner and outer vorticity centres (Figure 8(c)), and the asymmetry is able to draw energy continuously from the basic flow in a linear sense. It is this positive feedback that leads to the barotropic instability of the symmetric mean flow in TC1. The analytic eigenvalue solution for a piecewise-constant vorticity profile by Schubert *et al.* (1999) showed how the inner and outer disturbances located near the two jumps of

their vorticity profile would move in opposite directions, as shown in our phase and vorticity diagrams.

The overall pattern and evolution of the asymmetric vorticity and kinetic energy in TC3 are very similar to those in TC1 except that the growth rates are smaller (Figure 4). The non-dimensional growth rate for the wave-number two perturbation in TC3 is 0.16 (corresponding to an e-folding time-scale of 148 hours), which is consistent with the eigenvalue analysis but significantly smaller than that in TC1. The weaker instability in TC3 is attributed to the larger distance between the inner region of negative vorticity gradient and the outer region of positive vorticity gradient. This greater distance leads to a weaker mutual amplification of the inner and outer asymmetries through perturbation winds acting on the basic-state vorticity gradient.

4. Nonlinear barotropic model simulations

While the linear experiments above illustrate how the instability occurs, they do not allow the change of perturbations feeding back to the symmetric vortex. In this section, we examine how the evolution of asymmetric perturbation impacts the symmetric vortex in a nonlinear barotropic model. The governing equations for a nonlinear non-dimensional non-divergent barotropic model on an *f*-plane may be written as:

$$\left. \begin{aligned} \frac{\partial u}{\partial t} + u \frac{\partial u}{\partial x} + v \frac{\partial u}{\partial y} - v &= -\frac{\partial \phi}{\partial x}, \\ \frac{\partial v}{\partial t} + u \frac{\partial v}{\partial x} + v \frac{\partial v}{\partial y} + u &= -\frac{\partial \phi}{\partial y}, \\ -2J(u, v) - \zeta &= -\nabla^2 \phi, \end{aligned} \right\} \quad (4.1)$$

where $J(u, v) = \frac{\partial u}{\partial x} \frac{\partial v}{\partial y} - \frac{\partial v}{\partial x} \frac{\partial u}{\partial y}$ and $\zeta = \frac{\partial v}{\partial x} - \frac{\partial u}{\partial y}$.

The same initial condition as in the linear cases is used. The diagnostics for the energy exchange is made with the following symmetric KE equation:

$$\begin{aligned} \frac{\partial \bar{K}}{\partial t} &= -\frac{\partial(r\bar{u}\bar{K})}{r\partial r} - \bar{u} \frac{\partial(r\bar{u}'^2)}{r\partial r} - \bar{v} \frac{\partial(\bar{u}'\bar{v}')}{\partial r} \\ &+ \bar{u} \frac{\bar{v}'^2}{r} - \frac{2\bar{v}}{r} \bar{u}'\bar{v}' - \bar{u} \frac{\partial \bar{\phi}}{\partial r}, \end{aligned} \quad (4.2)$$

where the first term on the right-hand side of (4.2) is the flux divergence of \bar{K} by the symmetric radial flow, the sum of the second, third, fourth and fifth terms represents the symmetric KE change by wave-wave interactions, and the sixth term is the energy conversion from the symmetric potential energy into the symmetric kinetic energy. The first and the last terms on the right-hand side are not related to the energy transfer between the asymmetry and the symmetry.

Figure 9 shows the evolution of the asymmetric vorticity, the symmetric vorticity gradient, the symmetric kinetic energy and the total energy transfer between the symmetric and asymmetric flows in TC1. The initial wave-number two perturbation in the outer region ($r = 0.6$)

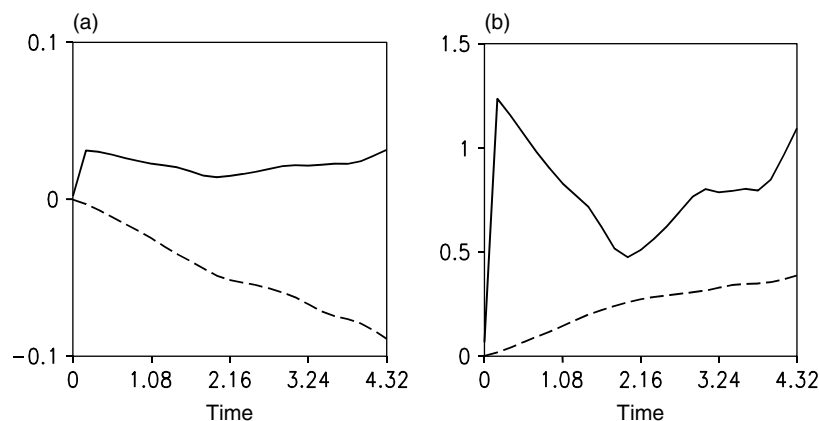


Figure 7. Evolution of the non-dimensional (a) asymmetric radial wind at the inner ($r = 0.3$, solid line) and outer ($r = 0.6$, dashed line) maximum asymmetric vorticity centres, (b) vorticity advection by the asymmetric flow ($-u'\partial\xi/\partial r$) in linear experiment for TC1.

grows until $t = 2.16$ and weakens slightly afterwards, while the inner asymmetric perturbation induced by the outer asymmetry continues to grow until $t = 3.24$ and then remains quasi-steady (Figure 9(a)). Compared to the linear case, the reduced growth rates in both the inner and outer regions are attributed to the modification of the symmetric vorticity gradient (Figure 9(b)), as the increased distance between the inner negative vorticity gradient centre and the outer positive vorticity gradient centre leads to a weaker instability. As the inner asymmetry grows, the symmetric kinetic energy and tangential wind near the radius of maximum wind decrease with time (Figure 9(c)). The symmetric KE change by wave–wave interactions is given in Figure 9(d). The diagnosis of the symmetric energy budget shows that the symmetric flows transfer kinetic energy to the asymmetric perturbations in the inner core region due to the up-shear tilt of the asymmetry (figure not shown). Such an energy transfer becomes weaker as the symmetric positive vorticity gradient centre shifts outwards.

Only the rate of energy transfer is shown for TC2 and TC3 (Figure 10). The symmetric flows transfer energy to the asymmetric perturbations before $t = 1.62$ (when the up-shear tilt is present), and gain energy from the asymmetric perturbation afterwards as the asymmetry changes its phase to a down-shear tilt (Figure 10(a)). Details of this can be found in Peng *et al.* (2008). The time evolution of the energy exchange in TC3 is very similar to the one in TC1, but weaker in magnitude (Figure 10(b)).

Figure 11 shows quantitatively to what extent the symmetric vortex intensity is influenced by the imposed initial asymmetric perturbation for wind profiles TC1, TC2 and TC3 after 24 h. For easier comparison, the maximum tangential wind has been normalized so that the weakening rate can be readily estimated. It turns out that the intensity reduction rate in TC1 is about three times as large as that in TC2, whereas the weakening rate in TC3 is about twice as large as in TC2.

The amplitude of the initial perturbation in the aforementioned experiments is modest ($A = 0.5$, a perturbation vorticity that is 7.4% of the basic-state maximum

vorticity). Two additional experiments with $A = 1.0$ and $A = 1.5$ are conducted to examine the sensitivity to amplitude of the initial perturbations. Figure 12 depicts the evolution of the maximum tangential wind in the control and the two new sensitivity experiments. While the maximum tangential wind decreases by 6% in the control experiment by 24 hours, a twice (three-times) larger initial asymmetric perturbation causes the decrease of the symmetric wind amplitude by 11% (18%) within 18 (12) hours. Therefore, the stronger the initial asymmetric perturbation is, the weaker the unstable symmetric vortex TC1 becomes. It is interesting to note that the TC1 vortex has its maximum wind increased after time 2.2 with the large initial asymmetry (Figure 12, dash-dotted line). In that case, the vortex is intensified by the much induced asymmetry near the RMW. However, the overall maximum tangential wind decreases with time due to the unstable growth of the asymmetry in the early stage.

5. Three-dimensional model simulations

We further examine three-dimensional simulations using the dry dynamics of the Weather Research and Forecast model (WRF), version 2.2. A horizontal grid spacing of 5 km is applied for a domain of 2000 km by 2000 km. The model extends to 10 hPa with 28 vertical sigma levels. The initial thermal profile is a mean tropical sounding, the same as the one used in Li *et al.* (2006). Diabatic physics processes in the model (such as convective and radiation) are turned off. The model is integrated for 48 hours at a time step of 15 s. The Coriolis parameter is set to be a constant $f = 5 \times 10^{-5} \text{ s}^{-1}$ at 20°N , the same as in the previous barotropic simulations. The upper and lower boundaries are free slip, and the lateral boundaries are fixed at their initial values.

The three-dimensional (3D) model was initialized with the balanced unstable vortex TC1 or stable vortex TC2 at the surface, decreasing to zero at the top model level (Li *et al.*, 2006). A wave-number two perturbation, with its maximum located at the radius of 600 km, is specified initially as in the barotropic simulations. The

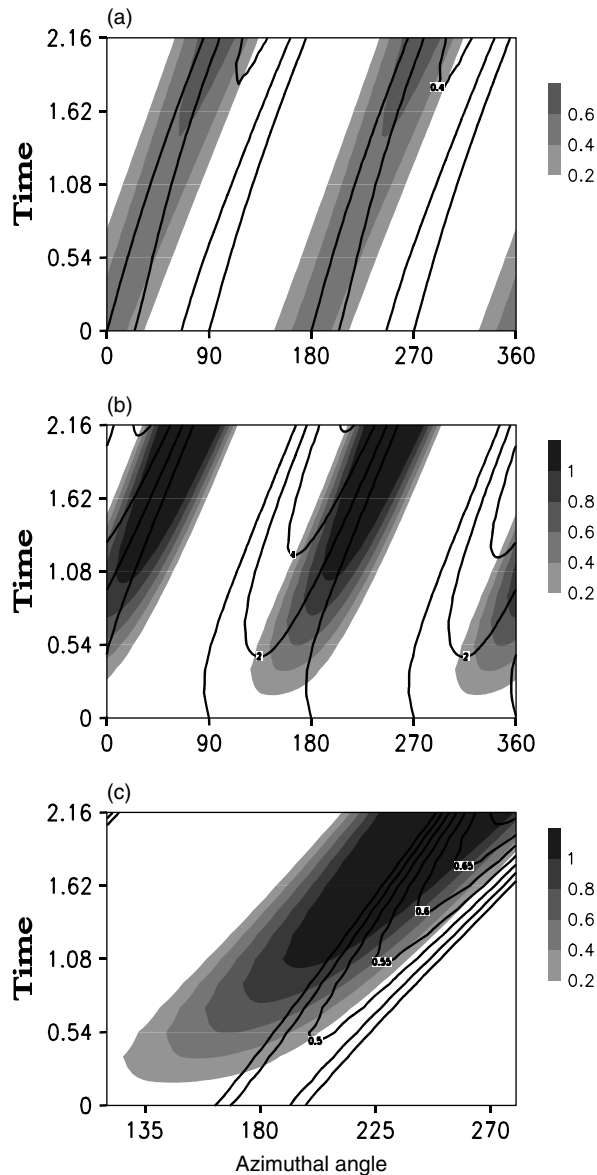


Figure 8. The time–azimuth cross-section of the wave-number two vorticity (positive only, shaded) and the vorticity tendency associated with the asymmetric radial wind advection (contour) at (a) $r = 0.6$ and (b) $r = 0.3$. The bottom panel (c) shows the phase relationship between the inner ($r = 0.3$, shaded) and outer ($r = 0.6$, contour) maximum asymmetric vorticity perturbations in linear experiment for TC1.

maximum wind of the asymmetric perturbation is 10% of the symmetric mean flow.

Figure 13 shows the evolution of the wave-number two perturbation at hours 0, 3, 9 and 18 in TC1. Similar to the 2D simulations, an inner-core asymmetry is generated by the initial perturbations in the outer region and there is phase lock between the inner asymmetry and the outer asymmetry. The interaction between the inner and the outer asymmetric perturbation causes the perturbations to continue gaining energy from the symmetric mean flow. The inner asymmetry grows much faster than the outer one, in agreement with the barotropic experiments.

For the stable vortex TC2, an inner-core asymmetry is also triggered by the initial outer asymmetry. It grows

during the first 9 hours and then weakens afterwards (figure not shown). No unstable development of asymmetric perturbations is observed in this experiment, as expected. The time evolution of the normalized maximum symmetric tangential wind in the two experiments is shown in Figure 14. A larger change of the mean vortex occurs in the unstable wind profile TC1 that agrees with the non-linear barotropic model result shown in Figure 11, but the overall changes of the symmetric winds are smaller in the 3D simulations.

6. Disturbances at different initial positions

Peng *et al.* (2008) shows that the impact of an asymmetric disturbance on a stable vortex through axisymmetrization depends critically on where the asymmetry is located initially. So far, we have investigated the instability with the initial perturbations specified in the outer region near where the basic-state vorticity gradient changes sign. What happens if the initial perturbations are placed at other locations? Two additional linear experiments for the basic vortex TC1 are carried out to answer this question. Experiment TC1L03 has the initial wave-number two perturbations located at the radius of 0.3 where the maximum vorticity gradient resides. In experiment TC1L45, the initial asymmetry is placed at radius 0.45, between the radii of maximum vorticity gradient. The evolution of the asymmetric vorticity amplitude and asymmetric kinetic energy for these two experiments are shown in Figure 15. The initial asymmetric perturbation in experiment TC1L03 propagates slightly outward, while additional asymmetry is induced inside the initial asymmetry (Peng *et al.*, 2008). In addition, new asymmetry grows in the outer region where local vorticity gradient has its second maximum. As the outer asymmetry grows, asymmetry near the inner radius of maximum vorticity gradient also grows through the feedback process as discussed for TC1. In TC1L45, even though the initial disturbance is placed between the inner and outer local (absolute) vorticity gradient maxima, the growth of the asymmetry is still concentrated at the two locations with large local vorticity gradient and the phase lock keeps the total asymmetry growing at the expense of the asymmetric part.

Putting all three experiments, TC1, TC1L03 and TC1L45 (Figures 4(d), 15(b) and 15(d)), into perspective, it becomes clear that all three have very similar behaviour, irrespective of the different positions of their initial asymmetry. As expected, asymmetries grow largest where the local basic-state vorticity gradient is largest (in an absolute sense). Because of the change of sign from one local vorticity gradient maximum to another, the asymmetries have a phase lock and grow under the instability.

7. Vortex with a smaller radius

The basic profiles we have examined so far are designed based on the NOGAPS model analysis, which has a

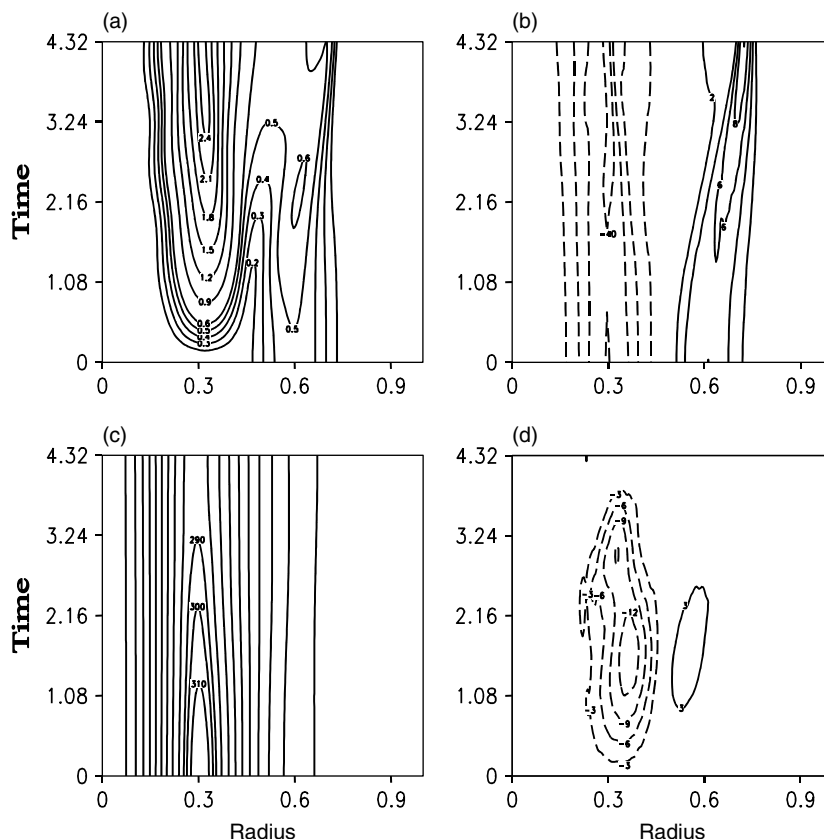


Figure 9. The time–radius cross-section of (a) the asymmetric vorticity amplitude, (b) the symmetric vorticity gradient, (c) the symmetric kinetic energy and (d) the rate of energy transfer from the asymmetric to symmetric flows in the nonlinear barotropic simulation for TC1.

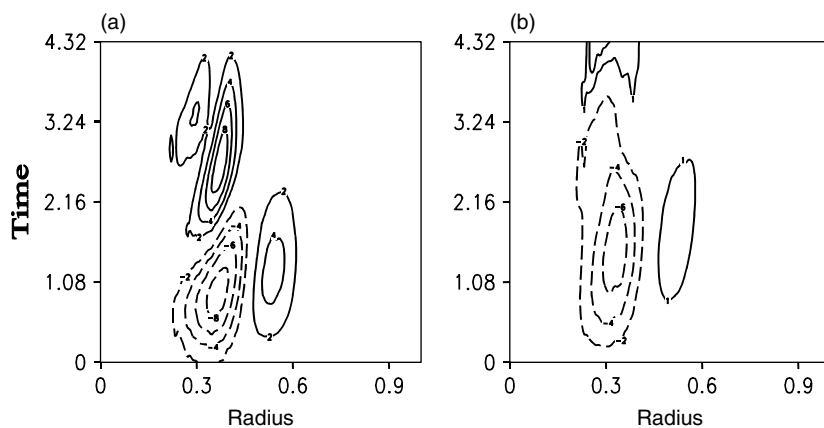


Figure 10. The time–radius cross-section of the rate of energy transfer from the asymmetric to symmetric flows in the nonlinear barotropic simulations for (a) TC2 and (b) TC3.

coarse resolution, and the TC profile typically has a large radius of maximum wind (200–300 km). To ensure the generality of our results, another unstable tropical cyclone profile is investigated. TC4 has its maximum tangential wind 0.5 (dimensional value, 25 m s^{-1}) located at the radius of 0.1 (100 km). The negative vorticity-gradient centre is situated at the radius of 0.1 while the positive vorticity-gradient centre is located at 0.25 (see Figure 16).

The initial perturbations are also given by (3.2) with the amplitude $A = 0.5$ and their maximum centre located at $r = 0.25$. Both linear and nonlinear experiments are

carried out, in comparison with the results from the unstable TC1. The initial perturbations located at $r = 0.25$ grow slowly till time 2.16, and decay afterwards in the linear simulation (Figure 17(a)). Meanwhile, the inner asymmetric perturbations are generated and intensify quickly to their maximum around time 1.0 and then weaken. While the asymmetries grow along the radius of local vorticity gradient extremes as seen in TC1 (Figure 9), the inner asymmetry grows much faster than the outer asymmetry in TC4 as the basic-state vorticity gradient near the radius of the maximum wind in TC4 is greater than that in TC1. The asymmetric component

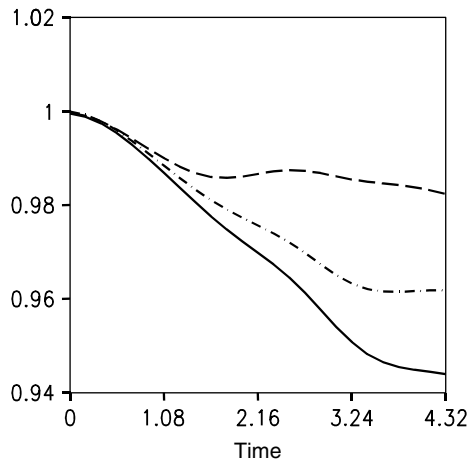


Figure 11. Evolution of normalized maximum tangential winds in the nonlinear barotropic simulations for TC1 (solid line), TC2 (dashed line) and TC3 (dash-dotted line).

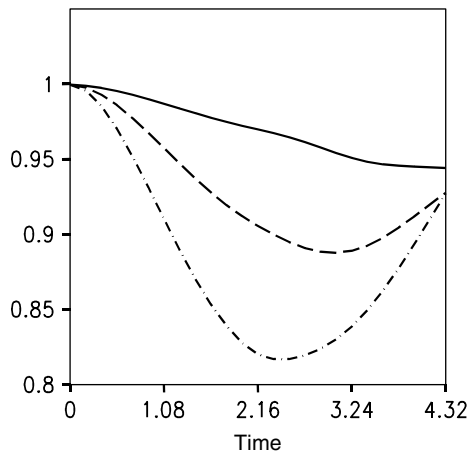


Figure 12. Evolution of normalized maximum tangential winds in nonlinear barotropic experiments for TC1 with the initial perturbation amplitude $A = 0.5$ (solid line), $A = 1.0$ (dashed line) and $A = 1.5$ (dash-dotted line).

in the nonlinear experiment has similar structure to that in the corresponding linear experiment (not shown). The maximum tangential wind of TC4 decreases with time as the energy is being transferred from the symmetric flows to the asymmetric perturbations, similar to the intensity change in TC1 (Figure 17(b)). Overall, the characteristics of the flow pattern in TC4 are very similar to those in TC1.

8. Conclusion and discussion

Much effort has been devoted to understanding vortex instability near the radius of maximum wind. The singular vector analysis by Peng and Reynolds (2006) indicates that intensity forecasts of TCs are most sensitive to the initial state in the outer region of a storm (around the radius of 500 km) where the vorticity gradient changes sign. As the wind associated with a storm merges with the environmental wind, it is not uncommon to find uneven vorticity gradient distribution along the radial direction

in the outer part of a storm, as observed in the daily analysis. In this study, we investigate the importance of the existence of the vorticity gradient sign change in the outer part of a TC-like vortex. Does this necessary condition support vortex instability? How does this type of unstable wind profile affect the development of the asymmetric perturbation and its interactions with the symmetric flow? We investigate these problems with linear and nonlinear barotropic models and a three-dimensional primitive equation model (WRF).

Three types of TC-like vortices (TC1, TC2 and TC3) are designed to mimic the observed stable and unstable wind profiles in the TC outer region, where TC1 and TC3 are strong and weak unstable vortices and TC2 is a stable vortex. Comparing to TC1, there is a larger distance between the inner negative vorticity gradient centre and the outer positive vorticity gradient centre in TC3.

The eigenvalue analysis reveals that wave-number two is the most unstable azimuthal mode in TC1 and TC3, with a non-dimensional growth rate measured by e-folding time-scales of 26 hours and 215 hours, respectively. No unstable modes appear in TC2, as expected.

The linear non-divergent barotropic model is used to investigate how the instability occurs. In both the unstable and stable cases, an inner asymmetric perturbation is induced by the initially specified outer asymmetry imposing on the basic-state vorticity gradient. The newly generated inner asymmetry feeds back to the growth of the outer symmetry in the unstable case through the basic-state vorticity gradient in the outer region. The increase of the outer asymmetry further enhances the growth of the inner asymmetry. Because of this mutual interaction, the vorticity advection by the asymmetric radial wind speeds up the phase propagation of the outer asymmetry while slowing down the phase propagation of the inner asymmetry. This process acts against the down-shear tendency effect by the differential symmetric mean flow advection (Montgomery and Kallenbach, 1997; Peng *et al.*, 2008) and allows the inner and the outer asymmetries to maintain an up-shear tilt by locking their phase line, connected between the inner and outer asymmetries. The up-shear tilt of the asymmetric vorticity causes energy transfer continuously from the symmetric mean flow to the asymmetric disturbances, thus the instability. In the stable case, the inner asymmetry cannot amplify the outer asymmetry because there is no basic-state vorticity gradient with a different sign in the outer part of the vortex. Therefore the initial up-shear tilt quickly shifts to a down-shear tilt by the differential basic-state tangential wind. This leads to the perturbation energy flowing back to the symmetric mean flow at a later stage, and the asymmetric perturbation decays. In TC3, there is a larger distance between the inner negative-vorticity-gradient centre and the outer positive-vorticity-gradient centre so that the positive feedback between the inner and the outer asymmetries is smaller, thus a weaker instability.

For the same given unstable radial wind profile (TC1), initial perturbations located at different radial positions

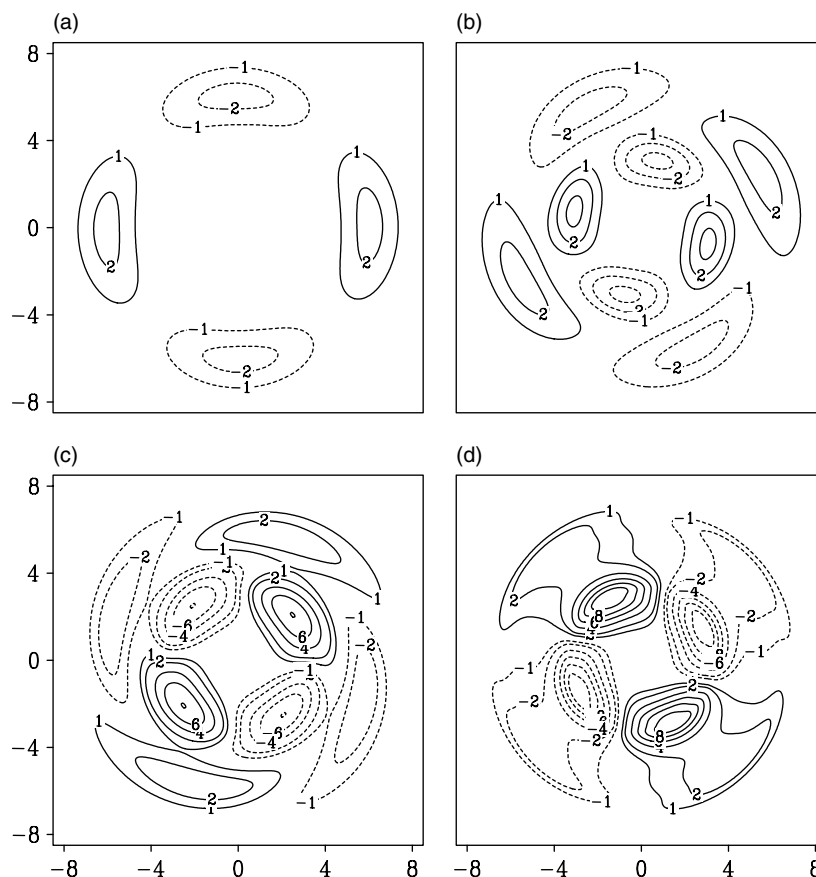


Figure 13. The wave-number two vorticity fields at time (a) 0 h, (b) 3 h, (c) 9 h and (d) 18 h in the WRF model experiment for TC1. The vorticity unit is 10^{-5} s^{-1} and the horizontal scale is 100 km.

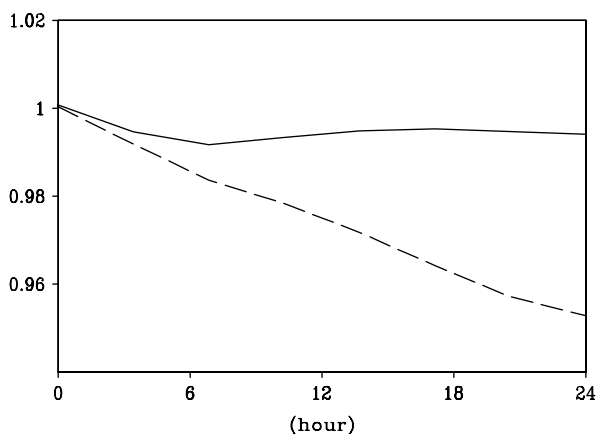


Figure 14. The temporal change of the normalized maximum tangential winds in the WRF model experiments for TC1 (dashed line) and TC2 (solid line).

result in similar growth of the asymmetry and similar evolution of the symmetry. This is due to the fact that, irrespective of the position of the initial disturbance, new asymmetries would always be induced where there is a basic-state vorticity gradient. When the basic-state vorticity gradient changes sign somewhere, the inner and the outer asymmetries can evolve in a lock-in phase tilt and maintain the instability. It is the profile of the basic-state vorticity gradient that determines the outcome of

the imposed asymmetry, not its position. This is very different for a stable profile in which the position of the initial asymmetry plays a critical role in determining the outcome (Peng *et al.*, 2008).

The impact of an initially specified asymmetric perturbation on the symmetric vortex is examined in a nonlinear barotropic model. The growing of the asymmetric perturbation weakens the symmetric vorticity gradient and reduces the barotropic instability gradually. The unstable growth of the asymmetric perturbation in TC1 can lead to a significant reduction of the symmetric vortex, depending on the magnitude of the initial disturbance. The 3D simulations are similar to the results from the nonlinear barotropic model.

Previous studies such as Montgomery and Kallenbach (1997) suggest that axisymmetrization may be an important mechanism that will feed energy from asymmetries to symmetric basic-state and increase the maximum intensity or outer part of the wind profile for a TC-like vortex (Peng *et al.*, 2008). The present study suggests that the existence of instability in the outer part of the wind profile (though it may be very weak) can cause a significant weakening of the basic-state vortex. Nolan *et al.* (2007) suggested that asymmetric heat sources would lead to eventual weakening of the symmetric wind in most situations with a stable profile. Therefore a TC-like vortex may require continuing injection of energy from convection to maintain and enhance its intensity.

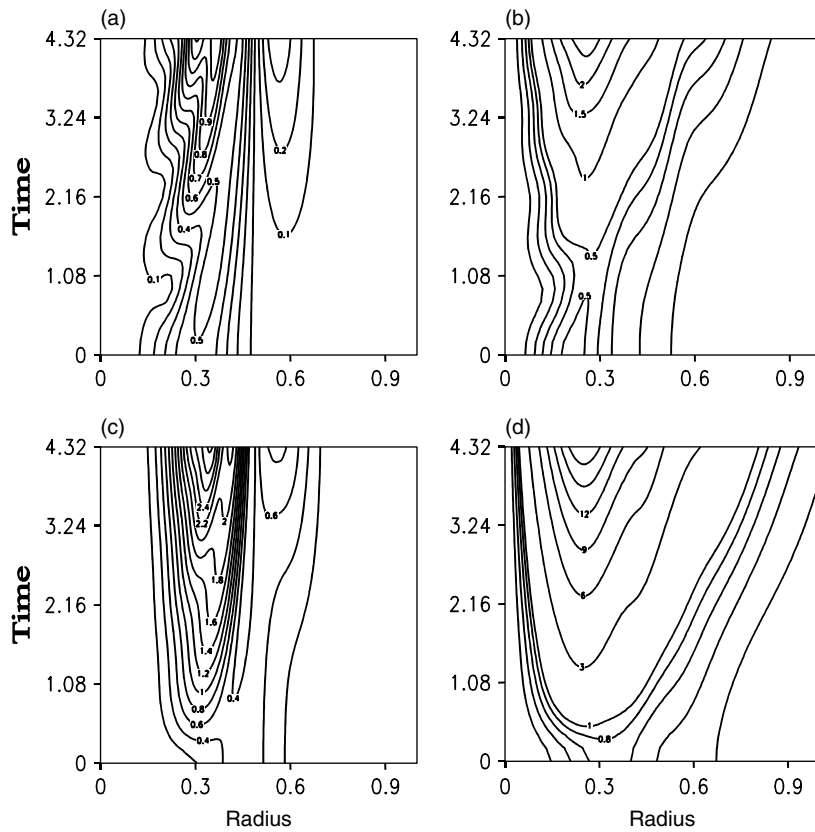


Figure 15. The time evolution of the asymmetric vorticity amplitude (a), (c) and asymmetric kinetic energy (b), (d) in vortex TC1 with the initial asymmetric perturbations located at the radius of 0.3 (0.45).

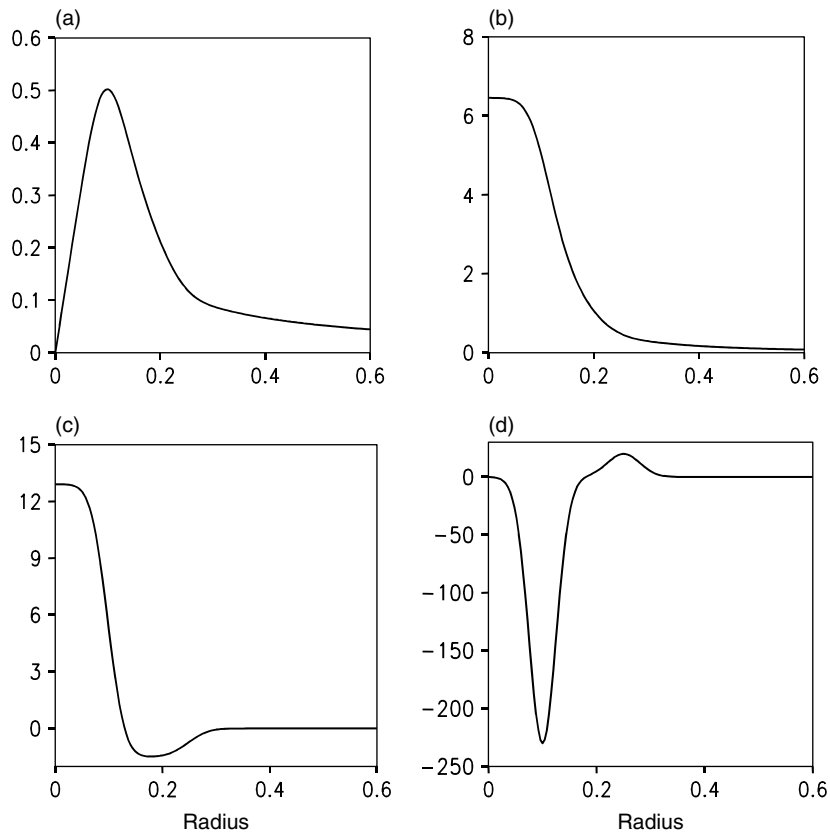


Figure 16. Radial profiles of the idealized vortex for non-dimensional (a) tangential wind, (b) angular velocity, (c) vorticity and (d) vorticity gradient for TC4.

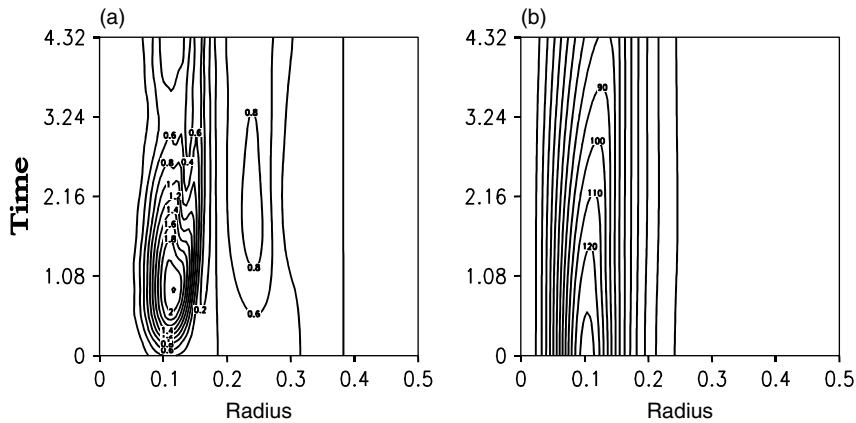


Figure 17. The temporal evolution of the (a) asymmetric vorticity amplitude in the linear experiment for TC4 and (b) symmetric kinetic energy in the nonlinear experiment for TC4.

Acknowledgements

This work was supported by ONR grants N000140710145, N000140810256, N00173061G031, PE 0602435N and NSFC Grants 40628006/40675054. The International Pacific Research Center is sponsored by the Japan Agency for Marine–Earth Science and Technology (JAMSTEC), NASA (NNX07AG53G) and NOAA (NA17RJ1230). This is SOEST contribution number 7638 and IPRC contribution number 588.

References

- Black ML, Willoughby HE. 1992. The concentric eyewall cycle of hurricane Gilbert. *Mon. Weather Rev.* **120**: 947–957.
- Gent PR, McWilliams JC. 1986. The instability of barotropic circular vortices. *Geophys. Astrophys. Fluid Dyn.* **35**: 209–233.
- Kossin JP, Schubert WH. 2001. Mesovortices, polygonal flow patterns, and rapid pressure falls in hurricane-like vortices. *J. Atmos. Sci.* **58**: 2196–2209.
- Kossin JP, Schubert WH, Montgomery MT. 2000. Unstable interactions between a hurricane's primary eyewall and a secondary ring of enhanced vorticity. *J. Atmos. Sci.* **57**: 3893–3917.
- Li T, Ge X, Wang B, Zhu Y. 2006. Tropical cyclogenesis associated with Rossby wave energy dispersion of a preexisting typhoon. Part II: Numerical simulations. *J. Atmos. Sci.* **63**: 1390–1409.
- Möller JD, Smith RK. 1994. The development of potential vorticity in a hurricane-like vortex. *Q. J. R. Meteorol. Soc.* **120**: 1255–1265.
- Montgomery MT, Kallenbach RJ. 1997. A theory for vortex Rossby waves and its application to spiral bands and intensity changes in hurricanes. *Q. J. R. Meteorol. Soc.* **123**: 435–465.
- Montgomery MT, Shapiro LJ. 1995. Generalized Charney–Stern and Fjortoft theorems for rapidly rotating vortices. *J. Atmos. Sci.* **52**: 1829–1833.
- Nolan DS, Grasso LD. 2003. Nonhydrostatic, three-dimensional perturbations to balanced, hurricane-like vortices. Part II: Symmetric response and nonlinear simulations. *J. Atmos. Sci.* **60**: 2717–2745.
- Nolan DS, Montgomery MT. 2000. The algebraic growth of wavenumber one disturbances in hurricane-like vortices. *J. Atmos. Sci.* **57**: 3514–3538.
- Nolan DS, Montgomery MT. 2002. Nonhydrostatic, three-dimensional perturbations to balanced, hurricane-like vortices. Part I: Linearized formulation, stability, and evolution. *J. Atmos. Sci.* **59**: 2989–3020.
- Nolan DS, Montgomery MT, Grasso LD. 2001. The wavenumber-one instability and trochoidal motion of hurricane-like vortices. *J. Atmos. Sci.* **58**: 3243–3270.
- Nolan DS, Moon Y, Stern DP. 2007. Tropical cyclone intensification from asymmetric convection: Energetics and efficiency. *J. Atmos. Sci.* **64**: 3377–3405.
- Peng MS, Reynolds CA. 2006. Sensitivity of tropical cyclone forecasts as revealed by singular vectors. *J. Atmos. Sci.* **63**: 2508–2528.
- Peng J, Peng MS, Li T. 2008. Dependence of vortex axisymmetrization on the characteristics of the asymmetry. *Q. J. R. Meteorol. Soc.* **134**: 1253–1268.
- Rayleigh L. 1880. On the stability, or instability, of certain fluid motions. *Proc. London Math. Soc.* **9**: 57–70.
- Schubert WH, Montgomery MT, Taft RK, Guinn TA, Fulton SR, Kossin JP, Edwards JP. 1999. Polygonal eyewalls, asymmetric eye contraction, and potential vorticity mixing in hurricanes. *J. Atmos. Sci.* **56**: 1197–1223.
- Shen TL, Tian YX, Ge XZ, Lu WS, Chen DH. 2003. *Numerical weather prediction*. Beijing Meteorology Press (in Chinese).
- Staley DO, Gall RL. 1979. Barotropic instability in a tornado vortex. *J. Atmos. Sci.* **36**: 973–981.
- Tervey WD, Montgomery MT. 2002. Wavenumber-2 and wavenumber- m vortex Rossby wave instabilities in a generalized three-region model. *J. Atmos. Sci.* **59**: 2421–2427.